Photochemical and Antimicrobial Properties of Novel C$_{60}$ Derivatives in Aqueous Systems

JAESANG LEE,[†] YURI MACKEYEV,[‡]
MIN CHO,[§] DONG LI,[†] JAE-HONG KIM,[§]
LON J. WILSON,[‡] AND
PEDRO J. J. ALVAREZ*,[†]

*Civil and Environmental Engineering, Rice University,
Houston, Texas 77005, Chemistry, Rice University,
Houston, Texas 77005, and Civil and Environmental
Engineering, Georgia Institute of Technology,
Atlanta, Georgia 30332*

Four novel hexakis C$_{60}$ derivatives with varying functionalities
were synthesized, and their photochemical properties and
photodynamic disinfection efficiencies were quantitatively
evaluated. All these C$_{60}$ derivatives generated $^1O_2$ more efficiently
than commercial multihydroxylated C$_{60}$ (fullerol), as assessed
by furfuryl alcohol consumption and electron paramagnetic
resonance analysis. Despite significant agglomeration/aggregation
in the aqueous phase to micrometer-sized particles, nanosecond
laser flash photolysis showed that the lifetime of triplet
state (a key intermediate for energy transfer responsible for
$^1O_2$ production) was comparable to reported values for pristine
C$_{60}$ in organic phase. As a result of facile $^1O_2$ production, the
C$_{60}$ derivatives efficiently inactivated *Escherichia coli* and MS-2
bacteriophage. Cationic aminofullerene hexakis, which likely
exerted electrostatic attraction, exhibited exceptionally rapid virus
inactivation even compared to commercial nano-TiO$_2$
photocatalyst. These unique photodynamic, hydrophilic and
cationic properties may be instrumental for the development
of next generation photocatalysts for disinfection applications.
The high ROS (reactive oxygen species) production activity
and associated cytotoxicity are concerns for potential releases
of functionalized C$_{60}$ to the environment, and require careful
assessment apart from other forms of C$_{60}$ (e.g., nC$_{60}$) that have
been widely studied as model nanomaterials but behave
differently.

Introduction

Remarkable energy and electron transfer properties of
photoexcited buckminsterfullerene (C$_{60}$) (*1−3*) have led to
various applications, including the development of novel
photoconductive (*4*), photoelectrochemical (*5*), and photo-
voltaic devices (*6*). In the presence of dissolved oxygen, energy
transfer from photoexcited triplet-state C$_{60}$ ($^3C_{60}$*) to triplet-
state oxygen ($^3O_2$) results in efficient production of singlet
oxygen ($^1O_2$) (*1, 7, 8*). $^3C_{60}$* can also be reduced to C$_{60}$ radical
anion (C$_{60}$$^{•-}$) by electron donors such as amines and alcohols

* Corresponding author phone: (713) 348-5903; fax: (713) 348-
5203; e-mail: alvarez@rice.edu.
† Civil and Environmental Engineering, Rice University.
‡ Chemistry, Rice University.
§ Georgia Institute of Technology.

(*2*), and subsequently reduce oxygen to superoxide radical
anion (O$_2$$^{-•}$) (*7, 9*). The efficient generation of these reactive
oxygen species (ROS) has been instrumental for photody-
namic therapy (*6, 10, 11*) and photosynthesis (*12*). However,
C$_{60}$'s extremely low water solubility has been a significant
challenge for the environmental and biomedical application
of its photoreactivity (*13*). C$_{60}$ can form stable colloidal
aggregates in water (i.e., nC$_{60}$) (*14*), but its intrinsic photo-
chemical properties are significantly lost due to aggregation
(*15−18*).

Functionalization of C$_{60}$ with hydrophilic moieties (*19, 20*)
is a promising approach to overcome its low aqueous
availability and prevent clustering that hinders energy and
electron transfer (*21*). Functionalized C$_{60}$ has been used in
medical and biological applications such as inhibition of
tumor growth (*22*), antiviral activity against the HIV-1 (*11*),
and selective DNA cleavage (*23*). At the same time, the
potential for the produced ROS to oxidize vital biological
constituents (*24*) and exert cytotoxicity (*23, 25*) is a concern
for potential releases of functionalized C$_{60}$ to the environment.
Nevertheless, these cytotoxic properties could be useful to
develop novel photocatalysts for water and wastewater
disinfection, which has not been examined thus far.

Badireddy et al. (*26*) recently demonstrated that ROS
produced by UV-irradiated fullerol (i.e., multihydroxylated
C$_{60}$ fullerene) readily inactivates MS-2 bacteriophage. Simi-
larly, C$_{60}$ oxides and hydroxides formed during ozone and
UV treatment of nC$_{60}$ exhibit enhanced photochemical
reactivity for $^1O_2$ generation (*27, 28*) and photoinduced
antibacterial activity (*29*). Brunet et al. (*15*) compared ROS
production by aqueous suspensions of fullerol, and PVP/C$_{60}$
(C$_{60}$ encapsulated with poly(*N*-vinylpyrrolidone)) vs TiO$_2$
(Degussa P25) nanoparticles. Under UV irradiation, nano-
TiO$_2$ produced •OH whereas C$_{60}$ derivatives produced $^1O_2$ in
ultrapure water and both $^1O_2$ and O$_2$$^{-•}$ in microbial growth
medium. When irradiated by an incandescent white lamp,
the efficiency for *Escherichia coli* disinfection was the highest
with PVP/C$_{60}$, followed by fullerol and nano-TiO$_2$. Whereas
such previous studies have yielded important information
on the photochemical and antimicrobial activities of selected
nanoparticles, these properties have not been quantitatively
evaluated for functionalized C$_{60}$ within the context of both
environmental applications and implications. This is a critical
knowledge gap considering the promising properties of
functionalized C$_{60}$ as a disinfection agent, including relatively
high aqueous availability (*19, 20*) and high photoreactivity
comparable to that of molecular C$_{60}$ (*21, 30*).

This study evaluates novel hexakis C$_{60}$ fullerenes (i.e.,
NH$_3$$^+$-, CO$_2$H-, or OH-terminated multifunctionalized C$_{60}$,
Table 1) as photoactive disinfectants relative to commercially
available fullerol and TiO$_2$ nanoparticles. Specifically, we
quantify their (1) photochemical reactivity, (2) inherent
potential cytotoxicity, and (3) photodynamic antimicrobial
activity.

Materials and Methods

Preparation of C$_{60}$ Derivatives. Hexakis C$_{60}$ derivatives were
synthesized using high purity (>99.9%) C$_{60}$ (MER) and
malonate analogues as described elsewhere (*19, 20*). Briefly,
nucleophilic addition of the malonate derivatives to double
bonds of C$_{60}$ was achieved using Bingel reaction (*31*) in
toluene in the presence of 1,8-diazabicyclo[5.4.0]undec-7-
ene (DBU) as a base. After functionalization, crude hexakis
adducts were isolated from the mixture of reaction products
using a liquid chromatography (LC). The resultant adducts
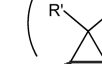underwent hydrolysis and subsequent conversion into hy-

TABLE 1. Chemical Structures of C$_{60}$ Derivatives

Chemical Structure	Abbreviation	R'	R''	Charge at pH 7
	HC1[a]	-CO$_2$H	-CO$_2$H	anionic
	HC2[b]	-CO$_2$H	(morpholine-N-carbonyl group)	anionic
	HC3[b]	-NHCH(CH$_2$OH)$_2$	-NHCH(CH$_2$OH)$_2$	neutral
	HC4[d]	-CO$_2$(CH$_2$)$_2$NH$_3^+$ CF$_3$CO$_2^-$	-CO$_2$(CH$_2$)$_2$NH$_3^+$ CF$_3$CO$_2^-$	cationic

[a] 1,2:18,36:22,23:27,45:31,32:55,60-hexakis[dicarboxy-methano]-1,2:18,36:22,23:27,45:31,32:55,60-dihydro[60]fullerene. [b] 3',3'',3''',3'''',3''''',3'''''''-hexa([1,4]oxazin-4-yl) 3'H,3''H,3'''H,3''''H,3'''''''H,3'''''''H-hexacyclopropa [1,2:18,36:22,23:27,45:31,32:55,60] (C$_{60}$-I$_h$)[5,6]-fullerene-3',3'',3''',3'''',3''''',3'''''''-hexacarboxylic acid. [c] 1,2:18,36:22,23:27,45:31,32:55,60-hexakis[di(2-hydroxy-1-hydroxymethyl-ethylcarbamoyl)-methano]-1,2:18,36:22,23:27,45:31,32:55,60-dihydro[60]fullerene. [d] 1,2:18,36:22,23:27,45:31,32:55,60-hexakis[di(2-aminoethyloxycarbonyl)-methano]-1,2:18,36:22,23:27,45:31,32:55,60-dihydro[60]fullerene, dodecatrifluoroacetate.

drophilic form, and were then purified by dialysis and dried in vacuum. The chemical structures and nomenclatures for these newly synthesized hexakis derivatives (designated as HC1, HC2, HC3, and HC4) are presented in Table 1. Supporting Information (SI) Figure S1 shows the UV–visible spectra of the C$_{60}$ derivatives. Fullerol (C$_{60}$(OH)$_{19-22}$(OK)$_4$) and TiO$_2$ (P25) were purchased from MTR Ltd. and Degussa, respectively.

Photochemical Activity. Experiments were performed using a magnetically stirred 60 mL cylindrical quartz reactor surrounded by six 4 W black light blue (BLB) lamps (emission wavelength region: 350–400 nm, Philips TL4W) at ambient temperature (22 °C), as previously described (*17, 18*). The incident light intensity in this active wavelength region was measured at 3.79×10^{-4} Einstein·min^{-1}L^{-1} by ferrioxalate actinometry (*32*). Reaction solutions containing 50 μM functionalized C$_{60}$ and 0.5 mM furfuryl alcohol (FFA) as an indicator for $^1O_2$ (*33*) [k(FFA + $^1O_2$) = 1.2×10^8 M^{-1}s^{-1} (*34*)] were buffered at pH 7 using 10 mM phosphate. As the photochemical reaction proceeded, sample aliquots of 1 mL were withdrawn from the reactor using a syringe, filtered through a 0.22 μm PTFE filter (Millipore), and injected into a 2 mL amber glass vial for further analysis. The residual FFA concentration at a constant time interval was measured using a HPLC (Waters 2695) equipped with a C-18 column (Nova-Pak C18) and a photodiode-array detector (Waters 996).

Electron Paramagnetic Resonance (EPR) Analysis. A Varian E-6 spectrometer was used under the following conditions: temperature = 293 K; microwave frequency = 9.225 GHz; microwave power = 10 mW; modulation amplitude = 1 G at 100 kHz; and scan time = 4 s and 2,2,6,6-tetramethyl-4-piperidinol (TMP) as a spin-trapping reagent for $^1O_2$ (*35*). The test solution (10 mM phosphate buffer at pH 7.0) consisted of 50 μM derivatized C$_{60}$ and 50 mM TMP. The solution was placed in a capillary glass tube and irradiated using one 4-W BLB lamp. The test tube was subjected to EPR measurement immediately after the light irradiation for 0 to 20 min during which $^1O_2$ rapidly oxidized TMP to 2,2,6,6-tetramethyl-4-piperidinol-*N*-oxyl radical (TMPN). Photosensitized $^1O_2$ generation by functionalized C$_{60}$ was evaluated by monitoring the EPR signal for TMPN.

Nanosecond Laser Flash Photolysis (LFP). To trace the decay kinetics of triplet states for hexakis C$_{60}$ derivatives, a 308 nm laser pulse (10–20 mJ, pulse width = 10 ns) from a Lambda Physik COMPex Excimer laser system was used as an excitation source and a xenon lamp as a monitoring source. The absorbance of all derivatized C$_{60}$ solutions (buffered at pH 7 with 10 mM phosphate) was adjusted at 0.5 at 308 nm, which lied in optimal regions for the LFP experiment. To inhibit energy transfer to oxygen, the test solution (3 mL) in a rectangular cell was vigorously bubbled with argon gas for 15 min and sealed from the atmosphere. Instantaneous generation of triplet state by laser pulse irradiation and the subsequent decay were monitored at a specific wavelength between 650 and 770 nm. The wavelength to monitor a triplet state was predetermined based on time-resolved spectrum of the triplet state of each derivative in the wavelength region from 425 to 800 nm, which displayed different spectral patterns depending on type of functional group (*30*).

Particle Size Determination. Suspensions of hexakis C$_{60}$ adducts and fullerol were analyzed by dynamic light scattering (DLS) using a Zetasizer Nano ZS90 with a detection limit of ca. 1 nm (Malvern Instruments, Worcestershire, OK) and, after drying on a carbon grid, a JEM 100C transmission electron microscope (TEM) (Jeol, Peabody, MA) with 100 kV electron beam.

Antibacterial Activity. Intrinsic antibacterial properties of selected hexakis derivatives and fullerol were evaluated in the dark using the minimum inhibitory concentration (MIC) assay with *Escherichia coli* K12 (ATCC no. 25404) as described by Lyon et al. (*36*). *E. coli* was cultured in Luria–Bertani (BD, Franklin Lakes, NJ) broth and incubated at 37 °C overnight prior to transferring to Minimal Davis (MD) media (i.e., Davis media with potassium phosphate reduced by 90%), and diluted to a final optical density at 600 nm (OD$_{600}$) of 0.002. C$_{60}$ derivatives were then added to the MD media at various concentrations. Overnight growth at 37 °C was assessed spectrophotometrically by measuring OD$_{600}$. The minimal concentration of functionalized C$_{60}$ resulting in no turbidity (indicating no growth of *E. coli*) was denoted as the MIC.

Photoinduced Bacterial and Viral Inactivation. Photoinduced bactericidal and virucidal activities of C$_{60}$ derivatives were assessed using *E. coli* (ATCC 8739) and MS-2 phage (ATCC 15597). *E. coli* was cultured in a tryptic soy broth (Difco Co., U.S.) for 18 h at 37 °C. The *E. coli* stock was prepared by resuspending the centrifuged harvest in 10 mM phosphate buffer after washing twice. The final concentration was determined by a spread plate method on nutrient agar after 24 h culture at 37 °C. The MS-2 phage was obtained by inoculating *E. coli* C3000 grown in the exponential to early stationary phase with MS-2 phage, and quantified by the soft agar overlay (double-agar layer) plaque assay method. MS-2 phage stock was prepared from overlay agar plates of confluent lysis as described elsewhere (*37*). Photosensitized microbial inactivation was performed using a BLB lamp with a light intensity low enough to ensure that UV irradiation alone did not induce any *E. coli* and MS-phage inactivation ($I = 8.4 \times 10^{-6}$ Einstein·min^{-1}L^{-1} for *E. coli*; $I = 6.1 \times 10^{-6}$

TABLE 2. Photosensitized $^1O_2$ Production in the Absence and Presence of Excess Scavengers

	initial FFA degradation rate[a] (μM/min) ($^1O_2$ production rate)		
C_{60} derivatives	no scavenger	L-histidine (50 mM)	t-BuOH (500 mM)
HC1	8.18 ± 0.68	0.15 ± 0.04	6.30 ± 0.44
HC2	13.28 ± 0.44	0.68 ± 0.10	11.68 ± 0.26
HC3	11.36 ± 0.56	0.72 ± 0.10	10.43 ± 0.92
HC4	19.06 ± 0.60	0.28 ± 0.13	18.21 ± 0.39
Fullerol	1.30 ± 0.19	0.25 ± 0.05	1.52 ± 0.14
Rose Bengal	16.34 ± 0.29	0.07 ± 0.04	16.70 ± 0.47

[a] Initial (20 min) degradation rate of FFA as $^1O_2$ indicator (measured in triplicate). Conditions: $[FFA]_0$ = 0.5 mM; $[phosphate]_0$ = 10 mM; $[C_{60}$ derivative$]_0$ = $[Rose Bengal]_0$ = 50 μM; pH 7.

Einstein·$min^{-1}L^{-1}$ for MS-phage). The reaction solutions (10 mM phosphate buffer at pH 7.0) for *E. coli* and MS-2 phage inactivation experiments consisted of 50 μM C_{60} derivative and either *E. coli* at 3×10^5 colony forming units (CFU)/mL or MS-2 phage at 3×10^5 plaque forming units (PFU)/mL, respectively. During each experiment, a 1 mL sample was withdrawn at fixed time intervals for quantification of *E. coli* and MS-2 phage. Three replicates analyses were performed (standard deviation <10%).

Results and Discussion

$^1O_2$ Production by C_{60} Derivatives. Table 2 shows significant $^1O_2$ production by C_{60} derivatives upon UV irradiation. FFA did not decay in the presence of UV alone or with C_{60} derivatives in the dark. Excess L-histidine (k(L-histidine + $^1O_2$) = 4.6 × 10^7 $M^{-1}s^{-1}$ (*34*)) drastically hindered FFA degradation, whereas excess t-BuOH as a •OH scavenger [k(FFA + $OH^•$) = 1.5 × 10^{10} $M^{-1}s^{-1}$ (*38*), k(t-BuOH + •OH) = 6 × 10^8 $M^{-1}s^{-1}$ (*39*)] did not significantly affect FFA degradation, both indicating that $^1O_2$ was the predominant ROS produced by these C_{60} derivatives. All novel C_{60} deriva-

tives exhibited much higher $^1O_2$ production rate than commercially available fullerol. The $^1O_2$ production rate was in the order of HC4 > HC2 > HC3> HC1. Functionalization could affect the photoreactivity of fullerenes in several ways, including (1) perturbation of the fullerene's conjugated π system, which is directly related to its photophysical properties, (2) modification of spectral properties relevant to photon absorption efficiency, and (3) change in degree of fullerene clustering, which influences triplet state decay kinetics as well as the surface area available for reaction. However, it is unknown how these effects collectively determine $^1O_2$ production, which precludes a mechanistic explanation for the observed trend and underscores the need for further research on fullerene structure—photoreactivity relationships.

Note that we used a polychromatic light source, which precludes determination of specific quantum yields. Nevertheless, we compared the kinetics of $^1O_2$ production by derivatized fullerenes with that of Rose Bengal, a widely used $^1O_2$ photosensitizer with a high quantum yield of 0.75 at 550 nm (*40*). The faster $^1O_2$ production rate by HC4 (hexakis C_{60} aminofullerene), and the similar rates observed for HC2 and HC3 (Table 2) indirectly shows the relatively high photoconversion efficiently of these fullerene derivatives.

EPR analysis confirmed the production of $^1O_2$ by derivatized C_{60} (Figure 1). The spectral intensity of TMPN, i.e., $^1O_2$ adduct with TMP, gradually increased as UV light was irradiated longer, and the kinetics of the EPR signal growth, indicative of $^1O_2$ production rate, was in the order of HC4 > HC2 > HC3 > fullerol, which was consistent with the above results.

Note that HC2 and HC4 effectively produced $^1O_2$ despite aggregating in aqueous phase to form relatively large particles (Table 3). This is in marked contrast to earlier findings that C_{60} aggregation (to nC_{60}) caused a drastic loss of its intrinsic photochemical properties (*16*–*18*). For instance, nC_{60} did not produce a detectable amount of $^1O_2$ under identical conditions (*17*). Compared to crystalline nC_{60} (*41*), HC2 clusters were amorphous and did not show any crystalline X-ray diffraction patterns during TEM analysis. Patches of HC4 particles indicated the presence of some crystalline
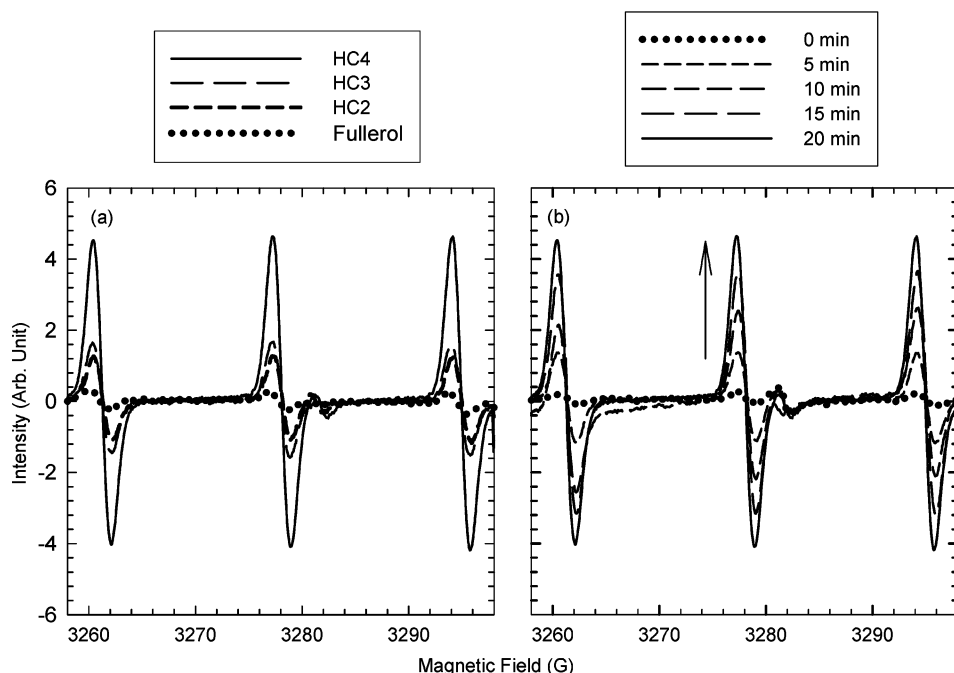

FIGURE 1. EPR spectra of TMP$-^1O_2$ adduct (TMPN) in aqueous suspensions of (a) selected derivatives (HC2, HC3, HC4, and Fullerol) after 20 min UV irradiation, and (b) HC4 as a function of irradiation time ($[C_{60}$ derivative$]_0$ = 50 μM; $[TMP]_0$ = 50 mM; $[phosphate]_0$ = 10 mM; pH$_i$ 7). Larger peaks correspond to higher $^1O_2$ generation.

TABLE 3. Minimal Inhibitory Concentration (MIC) Values and Average Particle Size of C$_{60}$ Derivatives

C$_{60}$ derivatives	MIC (μM)	average diameter (nm)
HC1	>400	1.32[a]/1.12[b]
HC2	>400	281.1/60.5
HC3	NA[c]	NA[c]
HC4	120	1.50/1,114
Fullerol	>400	2.43/6.10

[a] Determined with 50 μM functionalized C$_{60}$. [b] Determined with 50 μM functionalized C$_{60}$ in the presence of 10 mM phosphate buffer. [c] Not analyzed for anti-microbial properties due to insufficient availability of this material.

structures, but amorphous morphology was dominant (SI Figure S2). Unlike nC$_{60}$, HC2 and HC4 particle sizes were significantly affected by water chemistry, such as the presence of phosphate buffer (Table 3 and Figure 2). Overall, these results indicate that the formation of larger HC2 and HC4 particles might be related to amorphous aggregation or agglomeration of smaller primary particles (as is the case for the agglomeration of TiO$_2$ nanoparticles (42), (43)) rather than crystalline aggregation (as is the case for nC$_{60}$ (41)). Even if HC2 and HC4 formed aggregates, the bulky functional groups might have prevented direct contact between neighboring C$_{60}$ cage structures and subsequent effective quenching of triplet states, which is the primary reason for photoactivity loss by nC$_{60}$ (17, 18). Although further research is needed to elucidate how aggregate structure affects photochemical properties, the unexpectedly high photocatalytic activity of extensively aggregated/agglomerated derivatized C$_{60}$ could be very useful to develop solid phase catalysts (e.g., immobilization at a surface), to enable retention and recycling.

Evidence of Long-Lived Triplet States. The availability of transient triplet-state C$_{60}$ for energy transfer to oxygen is a key prerequisite for the production of $^1O_2$. The LFP results showed that the triplet state of derivatized C$_{60}$ was efficiently formed upon UV irradiation (Figure 3). The triplet-state production for all tested derivatives was much more efficient than fullerol, as evidenced by much larger absorption increase (at $t = 0$) from 625 to 770 nm. Under identical conditions, triplet state was not detected in nC$_{60}$, likely due to a rapid energy loss to neighboring C$_{60}$'s in the aggregates (18, 44).
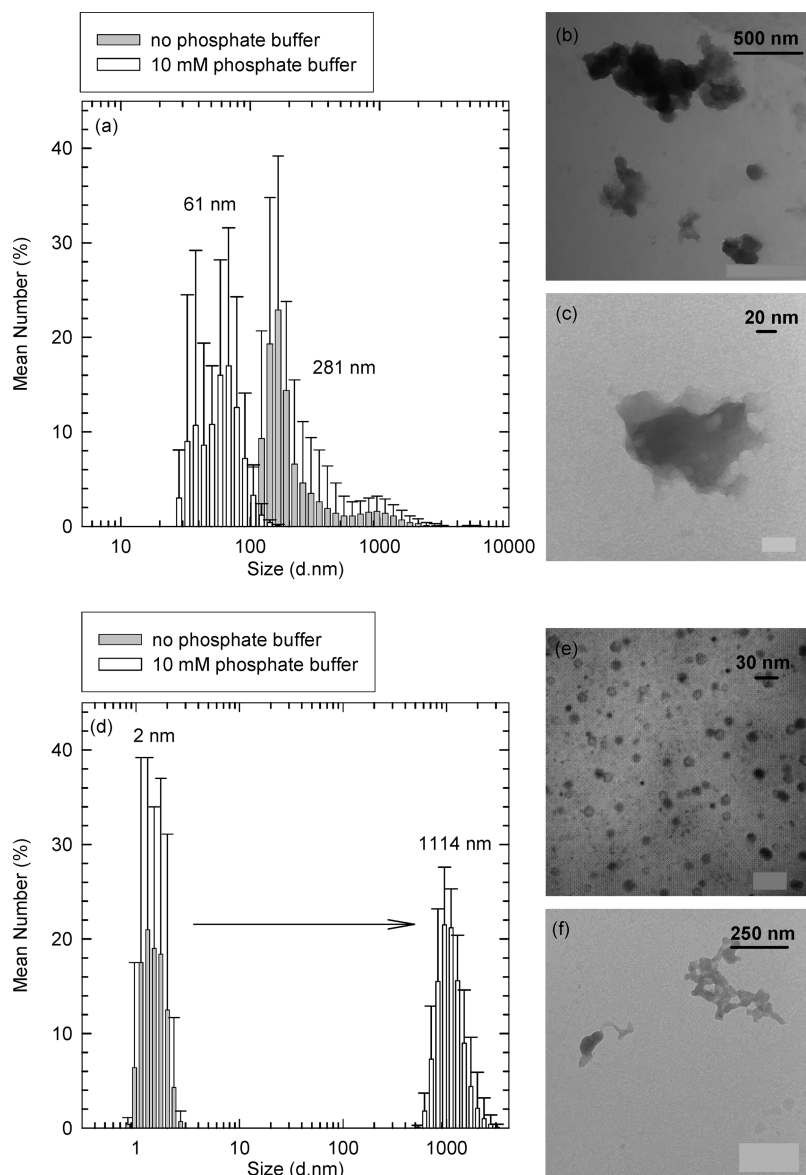

FIGURE 2. (a) DLS size distributions of HC2 and the TEM images in the **(b)** absence and **(c)** presence of 10 mM phosphate buffer, and **(d)** DLS size distributions of HC4 and the TEM images in the **(e)** absence and **(f)** presence of 10 mM phosphate buffer.

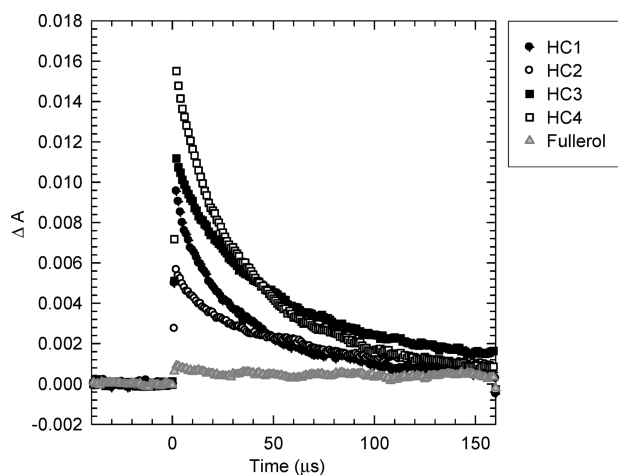**FIGURE 3. Decay profiles of triplet states recorded at 650−770 nm in aqueous suspensions of hexakis C_{60} derivatives and Fullerol (absorbance of C_{60} derivative = 0.5 at 308 nm; $[phosphate]_0$ = 10 mM; pH_i 7; Ar-saturated condition; λ (monitoring wavelength for triplet state) = 750 nm (HC1), 650 nm (HC2), 650 nm (HC3), 650 nm (HC4), 770 nm (Fullerol)).**
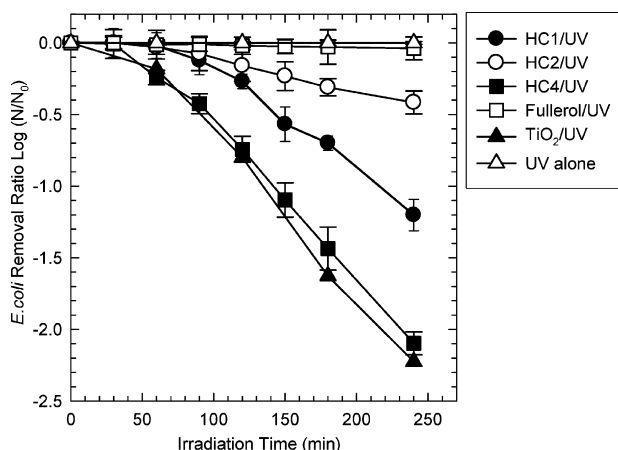

FIGURE 4. Comparison of photodynamic *E.coli* inactivation with hexakis C_{60} derivatives, Fullerol, and TiO_2 ($[C_{60}$ derivative$]_0$ = 50 μM ($[HC1]_0$ = 0.067 g/L; $[HC2]_0$ = 0.076 g/L; $[HC4]_0$ = 0.15 g/L; $[Fullerol]_0$ = 0.060 g/L); $[TiO_2]_0$ = 0.2 g/L; $[phosphate]_0$ = 10 mM; pH_i = 7).

The lifetime of the triplet state ranged from 30 to 44 μs for these novel C_{60} derivatives, which were not only much longer than fullerol (approximately 9 μs) but even comparable to pristine molecular C_{60} in hexane (*1*). Therefore, despite the formation of larger particles, these derivatized C_{60}'s retained the intrinsic energy transfer properties of pristine C_{60}, which is ultimately responsible for $^1O_2$ production in water.

Intrinsic Antibacterial Properties. Compared to nC_{60} (*E. coli* MIC ranging from 0.7 to 2.8 μM) (*45*), HC1, HC2, and fullerol did not inhibit *E. coli* growth in the dark (i.e., MIC > 400 μM) (Table 3), while HC4 inhibited *E. coli* growth at 120 μM. The antibacterial activity of HC4, although much milder than nC_{60}, might be partly attributed to the positively charged ammonium functional groups on this derivative, which could enhance surface interaction with negatively charged *E. coli* (*46*).

Photoinduced Bacterial Inactivation. Figure 4 compares inactivation kinetics of *E. coli* by hexakis C_{60} derivatives, fullerol, and TiO_2 (Degussa P25). No detectable *E. coli* inactivation was observed in the dark in all cases (data not shown), which corroborates the low to negligible intrinsic toxicity determined by the MIC test (Table 3). Significant *E. coli* inactivation by hexakis C_{60} derivatives was observed after a lag period that is
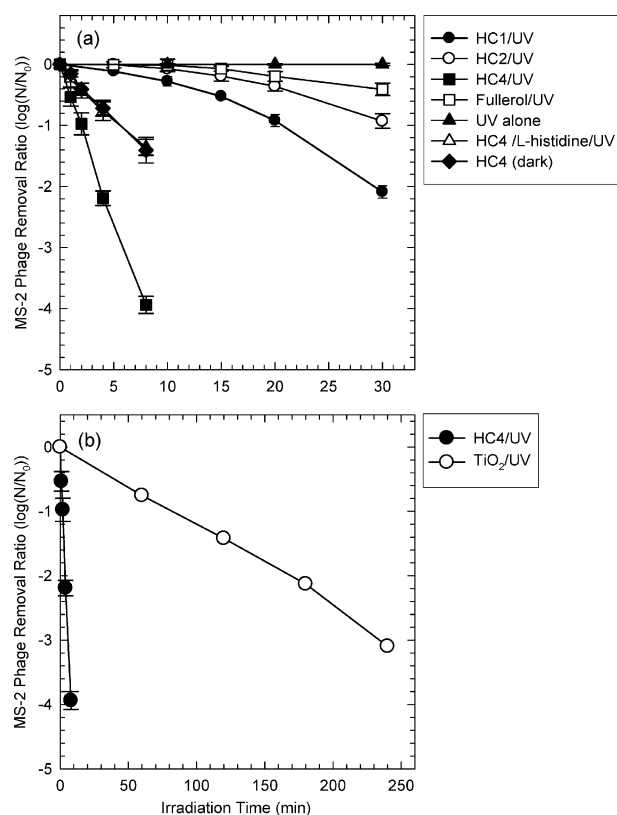

FIGURE 5. Comparison of (a) photodynamic MS-2 phage inactivation with hexakis C_{60} derivatives and Fullerol, and antiviral activity of HC4 derivative in the dark, and (b) with HC4 and TiO_2 photocatalyst ($[C_{60}$ derivative$]_0$ = 50 μM ($[HC1]_0$ = 0.067 g/L; $[HC2]_0$ = 0.076 g/L; $[HC4]_0$ = 0.15 g/L; $[Fullerol]_0$ = 0.060 g/L); $[L-histidine]_0$ = 50 mM; $[TiO_2]_0$ = 0.2 g/L; $[phosphate]_0$ = 10 mM; pH_i = 7).

typical for bacterial disinfection kinetics (*47, 48*). Under the tested conditions, no *E. coli* was inactivated by fullerol. When excess L-histidine as a $^1O_2$ scavenger was added, *E. coli* was not inactivated even with HC4 (SI Figure S3a), confirming that $^1O_2$ was the primary disinfecting agent. Among the tested C_{60} derivatives, HC4 ($[HC4]_0$ = 50 μM = 0.15 g/L) was as efficient as TiO_2 ($[TiO_2]_0$ = 0.2 g/L) for photocatalytic inactivation of *E. coli* (Figure 4).

Photoinduced Virus Inactivation. Photodynamic inactivation by C_{60} derivatives was much more efficient for MS-2 phage compared to *E. coli* (Figure 5a). This is particular noteworthy because virus are typically more resistant than bacteria in UV (*49*) and some photocatalytic disinfection processes (*48, 50*). The critical role of $^1O_2$ was also evident as MS-2 phage inactivation by HC4 (10 μM) was not observed in the presence of excess L-histidine (50 mM) (SI Figure S3b). However, when higher concentrations of HC4 were used (50 μM), MS-2 phage inactivation was observed even in the presence of excess L-histidine (50 mM) and under dark conditions. This corroborates the higher intrinsic antimicrobial property of HC4 inferred by the MIC analysis (Table 3). Although the dark inactivation mechanism is unclear, the high antimicrobial activity of HC4 could be related to its cationic nature promoting electrosorption (*10, 46*), and to the antibacterial activity exerted by quaternary ammonium compounds (QACs) (*51*). Viral inactivation by all C_{60} derivatives, HC4 in particular, was remarkably more efficient than commercial nano-TiO_2 photocatalyst (Figure 5b). Under identical conditions, 0.15 g/L of HC4 led to 2-log inactivation of MS-2 phage within only 4 min, whereas it took 3 h to achieve a similar inactivation level with 0.2 g/L of TiO_2.

Factors Affecting the Inactivation Kinetics. Although $^1O_2$ was identified as a primary agent, additional mechanisms seem to be involved in *E. coli* and MS-2 phage inactivation by C_{60} derivatives. Inactivation efficacy correlates well to $^1O_2$ production when HC4 and fullerol are compared. However, for anionic derivatives, HC1 was a more efficient inactivating agent than HC2 despite its slower $^1O_2$ production rate (Table 2). This could be partly explained by the smaller size of HC1 in the aqueous phase (near the size of single molecule) compared to HC2 (with significant aggregation/agglomeration). The smaller size results in higher surface active area to interact with bacteria and virus, and might facilitate HC1 penetration into bacterial cells to enhance inactivation efficiency. For example, a recent study suggested that hydroxylated C_{60} (produced from ozonation of nC_{60}) could readily penetrate into *E. coli* and produce ROS upon UV irradiation, leading to significantly enhanced toxicity (*29*).

The extraordinarily high antimicrobial activity of HC4 compared to other derivatives cannot be explained solely by its greater $^1O_2$ production rate. For example, 2 orders of magnitude faster inactivation of MS-2 phage was observed with HC4 compared to HC2 and fullerol, whereas the $^1O_2$ production rate was only 1.5−15 times greater, respectively. Furthermore, HC4 added at 5-fold lower concentration than other derivatives was more efficient in inactivating MS-2 phage (SI Figure S4). This suggests that electrostatic attraction between the cationic amine-functional groups of HC4 and the anionic *E. coli* and MS-phage surfaces might have facilitated reactions with short-lived $^1O_2$ (*e.g.*, lifetime of 2 μs in distilled water (*52*)). This notion is supported by findings that cationic porphyrin as a $^1O_2$ photosensitizer exerts much faster inactivation kinetics for *E. coli* (*53*) and bacteriophage (*54*) than anionic and neutral analogues with identical $^1O_2$ quantum yields.

Environmental Implications and Applications. This study demonstrated that novel hexakis C_{60} derivatives exhibit unique photochemical and antibacterial properties that are in marked contrast to those of nC_{60} and commercial fullerol. Among these derivatives, HC4 was as efficient as commercial nano-TiO_2 photocatalyst for *E. coli* disinfection, and much more efficient for MS-2 phage inactivation. These properties could be very valuable for the development of novel disinfecting agents, considering that (1) HC4 retains the intrinsic photochemical property of C_{60} despite significant agglomeration/aggregation, and (2) the availability of amine functional groups offers an opportunity for immobilization to solid media (such as a particle or surface) via covalent bonding, which would be more stable than physiosorption mechanisms used to immobilize TiO_2. Note that difficulties involved with recovering catalysts and gradual loss of catalysts from the surface have been limiting widespread application of many photocatalysts, including TiO_2, in large scale processes (*55*). Albeit, the distinct properties that encourage the increased use of such derivatized C_{60} photocatalysts in water or wastewater treatment also call for a proactive assessment of potential environmental impacts associated with incidental or accidental releases of such novel particles to natural water bodies. The size distribution, surface properties, and photochemical reactivity of these novel hexakis C_{60} derivatives are very different from those of widely studied nC_{60} and fullerol, and might therefore require special attention for handling and disposal.

Acknowledgments

Supporting Information Available

An additional Figure showing the UV-Visible spectra of the aqueous suspensions of C_{60} fullerene derivatives used in this work (Figure S1). Figure S2 is the X-ray diffraction on HC4 particles. Figure S3a and b depict the kinetics for photodynamic inactivation of *E. coli* and MS-2 bacteriophage by HC4 in the absence and presence of excess L-histidine as a $^1O_2$ scavenger. MS-2 bacteriophage inactivation by HC4 is depicted for varying initial concentrations of the tested C_{60} derivatives (Figure S4). This material is available free of charge via the Internet at http://pubs.acs.org.

Literature Cited

(1) Arbogast, J. W.; Darmanyan, A. P.; Foote, C. S.; Rubin, Y.; Diederich, F. N.; Alvarez, M. M.; Anz, S. J.; Whetten, R. L. Photophysical properties of C_{60}. *J. Phys. Chem.* **1991**, *95*, 11–12.

(2) Arbogast, J. W.; Foote, C. S.; Kao, M. Electron transfer to triplet C_{60}. *J. Am. Chem. Soc.* **1992**, *114*, 2277–2279.

(3) Fraelich, M. R.; Weisman, R. B. Triplet-states of C_{60} and C_{70} in solution - Long intrinsic lifetimes and energy pooling. *J. Phys. Chem.* **1993**, *97*, 11145–11147.

(4) Wang, Y.; Suna, A. Fullerenes in photoconductive polymers. Charge generation and charge transport. *J. Phys. Chem. B* **1997**, *101*, 5627–5638.

(5) Imahori, H.; Mitamura, K.; Shibano, Y.; Umeyama, T.; Matano, Y.; Yoshida, K.; Isoda, S.; Araki, Y.; Ito, O. A photoelectrochemical device with a nanostructured SnO_2 electrode modified with composite clusters of porphyrin-modified silica nanoparticle and fullerene. *J. Phys. Chem. B* **2006**, *110*, 11399–11405.

(6) Barber, R. P.; Gomez, R. D.; Herman, W. N.; Romero, D. B. Organic photovoltaic devices based on a block copolymer/fullerene blend. *Org. Electron.* **2006**, *7*, 508–513.

(7) Yamakoshi, Y.; Umezawa, N.; Ryu, A.; Arakane, K.; Miyata, N.; Goda, Y.; Masumizu, T.; Nagano, T. Active oxygen species generated from photoexcited fullerene (C_{60}) as potential medicines: $O_2^{\bullet-}$ versus $^1O_2$. *J. Am. Chem. Soc.* **2003**, *125*, 12803–12809.

(8) Orfanopoulos, M.; Kambourakis, S. Chemical evidence of singlet oxygen production from C_{60} and C_{70} in aqueous and other polar media. *Tetrahedron Lett.* **1995**, *36*, 435–438.

(9) Yamakoshi, Y.; Sueyoshi, S.; Fukuhara, K.; Miyata, N. $\cdot$OH and $O_2^{\bullet-}$ generation in aqueous C_{60} and C_{70} solutions by photoirradiation: An EPR study. *J. Am. Chem. Soc.* **1998**, *120*, 12363–12364.

(10) Jensen, A. W.; Wilson, S. R.; Schuster, D. I. Biological applications of fullerenes. *Bioorg. Med. Chem.* **1996**, *4*, 767–779.

(11) Kasermann, F.; Kempf, C. Buckminsterfullerene and photodynamic inactivation of viruses. *Rev. Med. Virol.* **1998**, *8*, 143–151.

(12) Jensen, A. W.; Daniels, C. Fullerene-coated beads as reusable catalysts. *J. Org. Chem.* **2003**, *68*, 207–210.

(13) Heymann, D. Solubility of fullerenes C_{60} and C_{70} in seven normal alcohols and their deduced solubility in water. *Fuller. Sci. Technol.* **1996**, *4*, 509–515.

(14) Deguchi, S.; Alargova, R. G.; Tsujii, K. Stable dispersions of fullerenes, C_{60} and C_{70}, in water. Preparation and characterization. *Langmuir* **2001**, *17*, 6013–6017.

(15) Brunet, L.; Lyon, D.; Hotze, E. M.; Alvarez, P. J. J.; Wiesner, M. R. Comparative photoactivity and antibacterial properties of C_{60} Fullerenes and titanium dioxide nanoparticles. *Environ. Sci. Technol.* 43 4355−4360.

(16) Hotze, E. M.; Labille, J.; Alvarez, P. J. J.; Wiesner, M. R. Mechanisms of photochemistry and reactive oxygen production by fullerene suspensions in water. *Environ. Sci. Technol.* **2008**, *42*, 4175–4180.

(17) Lee, J.; Fortner, J. D.; Hughes, J. B.; Kim, J.-H. Photochemical production of reactive oxygen species by C_{60} in the aqueous phase during UV irradiation. *Environ. Sci. Technol.* **2007**, *41*, 2529–2535.

(18) Lee, J.; Yamakoshi, Y.; Hughes, J. B.; Kim, J.-H. Mechanism of C_{60} photoreactivity in water: Fate of triplet state and radical anion and production of reactive oxygen species. *Environ. Sci. Technol.* **2008**, *42*, 3459–3464.

(19) Richardson, C. F.; Schuster, D. I.; Wilson, S. R. Synthesis and characterization of water-soluble amino fullerene derivatives. *Org. Lett.* **2000**, *2*, 1011–1014.

(20) Wharton, T.; Kini, V. U.; Mortis, R. A.; Wilson, L. J. New non-ionic, highly water-soluble derivatives of C_{60} designed for biological compatibility. *Tetrahedron Lett.* **2001**, *42*, 5159–5162.

(21) Guldi, D. M.; Prato, M. Excited-state properties of C_{60} fullerene derivatives. *Acc. Chem. Res.* **2000**, *33*, 695–703.

(22) Tabata, Y.; Murakami, Y.; Ikada, Y. Antitumor effect of poly-(ethylene glycol)modified fullerene. *Fuller. Sci. Technol.* **1997**, *5*, 989–1007.

(23) Tokuyama, H.; Yamago, S.; Nakamura, E.; Shiraki, T.; Sugiura, Y. Photoinduced biochemical activity of fullerene carboxylic acid. *J. Am. Chem. Soc.* **1993**, *115*, 7918–7919.

(24) Michaeli, A.; Feitelson, J. Reactivity of singlet oxygen toward amino acids and peptides. *Photochem. Photobiol.* **1994**, *59*, 284–289.

(25) Irie, K.; Nakamura, Y.; Ohigashi, H.; Tokuyama, H.; Yamago, S.; Nakamura, E. Photocytotoxicity of water-soluble fullerene derivatives. *Biosci. Biotechnol. Biochem.* **1996**, *60*, 1359–1361.

(26) Badireddy, A. R.; Hotze, E. M.; Chellam, S.; Alvarez, P. J. J.; Wiesner, M. R. Inactivation of Bacteriophages via photosensitization of fullerol nanoparticles. *Environ. Sci. Technol.* **2007**, *41*, 6627–6632.

(27) Lee, J.; Cho, M.; Fortner, J. D.; Hughes, J. B.; Kim, J.-H. , Transformation of aggregated C_{60} in the aqueous phase by UV irradiation. *Environ. Sci. Technol.*, 434878−4883.

(28) Fortner, J. D.; Kim, D. I.; Boyd, A. M.; Falkner, J. C.; Moran, S.; Colvin, V. L.; Hughes, J. B.; Kim, J. H. Reaction of water-stable C_{60} aggregates with ozone. *Environ. Sci. Technol.* **2007**, *41*, 7497–7502.

(29) Cho, M.; Fortner, J. D.; Hughes, J. B.; Kim, J.-H. , *Escherichia coli* inactivation by water soluble ozonated C_{60} derivative: Kinetics and mechanisms. *Environ. Sci. Technol.* Submitted.

(30) Guldi, D. M.; Asmus, K. D. Photophysical properties of mono- and multiply-functionalized fullerene derivatives. *J. Phys. Chem. A* **1997**, *101*, 1472–1481.

(31) Bingel, C. Cyclopropylation of fullerenes. *Chem. Ber.* **1993**, *126*, 1957–1959.

(32) Hatchard, C. G.; Parker, C. A. A new sensitive chemical actinometer 2. Potassium ferrioxalate as a standard chemical actinometer. *Proc. R. Soc. London, Ser. A* **1956**, *235*, 518–536.

(33) Haag, W. R.; Hoigné, J. Singlet oxygen in surface waters. 3. Photochemical formation and steady-state concentrations in various types of waters. *Environ. Sci. Technol.* **1986**, *20*, 341–348.

(34) Wilkinson, F.; Helman, W. P.; Ross, A. B. Rate constants for the decay and reactions of the lowest electronically excited singlet-state of molecular oxygen in solution−An expanded and revised compilation. *J. Phys. Chem. Ref. Data* **1995**, *24*, 663–1021.

(35) Lion, Y.; Gandin, E.; Vandevorst, A. On the production of nitroxide radicals by singlet oxygen reaction−An electron paramagnetic resonance study. *Photochem. Photobiol.* **1980**, *31*, 305–309.

(36) Lyon, D. Y.; Adams, L. K.; Falkner, J. C.; Alvarez, P. J. J. Antibacterial activity of fullerene water suspensions: Effects of preparation method and particle size. *Environ. Sci. Technol.* **2006**, *40*, 4360–4366.

(37) Debartolomeis, J.; Cabelli, V. J. Evaluation of an *Escherichia coli* host strain for enumeration of f-male-specific bacteriophages. *Appl. Environ. Microbiol.* **1991**, *57*, 1301–1305.

(38) Buxton, G. V.; Greenstock, C. L.; Helman, W. P.; Ross, A. B. Critical review of rate constants for reactions of hydrated electrons, hydrogen atoms and hydroxyl radicals in aqueous solution. *J. Phys. Chem. Ref. Data* **1988**, *17*, 513–886.

(39) Vonpiechowski, M.; Thelen, M. A.; Hoigne, J.; Buhler, R. E. Tert-butanol as an OH radical scavenger in the pulse-radiolysis of oxygenated aqueous systems. *Ber. Bunsen−Ges. Phys. Chem.* **1992**, *96*, 1448–1454.

(40) Muraseccosuardi, P.; Gassmann, E.; Braun, A. M.; Oliveros, E. Determination of the quantum yield of intersystem crossing of rose bengal. *Helv. Chim. Acta* **1987**, *70*, 1760–1773.

(41) Li, L. W.; Bedrov, D.; Smith, G. D. Water-induced interactions between carbon nanoparticles. *J. Phys. Chem. B* **2006**, *110*, 10509–10513.

(42) Fernández-Ibáñez, P.; Malato, S.; de las Nieves, F. J. Relationship between TiO_2 particle size and reactor diameter in solar photoreactors efficiency. *Catal. Today* **1999**, *54*, 195–204.

(43) Zhao, Y. J.; Zhang, Y.; Xing, W. H.; Xu, N. P. Influences of pH and ionic strength on ceramic microfiltration of TiO_2 suspensions. *Desalination* **2005**, *177*, 59–68.

(44) Lee, J.; Kim, J.-H. Effect of encapsulating agents on dispersion status and photochemical reactivity of C_{60} in the aqueous phase. *Environ. Sci. Technol.* **2008**, *42*, 1552–1557.

(45) Lyon, D. Y.; Fortner, J. D.; Sayes, C. M.; Colvin, V. L.; Hughes, J. B. Bacterial cell association and antimicrobial activity of a C_{60} water suspension. *Environ. Toxicol. Chem.* **2005**, *24*, 2757–2762.

(46) Tang, Y. J. J.; Ashcroft, J. M.; Chen, D.; Min, G. W.; Kim, C. H.; Murkhejee, B.; Larabell, C.; Keasling, J. D.; Chen, F. Q. F. Charge-associated effects of fullerene derivatives on microbial structural integrity and central metabolism. *Nano Lett.* **2007**, *7*, 754–760.

(47) Cho, M.; Lee, Y.; Chung, H.; Yoon, J. Inactivation of *Escherichia coli* by photochemical reaction of ferrioxalate at slightly acidic and near-neutral pHs. *Appl. Environ. Microbiol.* **2004**, *70*, 1129–1134.

(48) Cho, M.; Chung, H. M.; Choi, W. Y.; Yoon, J. Y. Different inactivation behaviors of MS-2 phage and *Escherichia coli* in TiO_2 photocatalytic disinfection. *Appl. Environ. Microbiol.* **2005**, *71*, 270–275.

(49) *Alternative Disinfectants and Oxidations: Guidance Manual*; U.S. Environmental Protection Agency: Washington, D.C., 1999.

(50) Kim, J. Y.; Lee, C.; Cho, M.; Yoon, J. Enhanced inactivation of *E. coli* and MS-2 phage by silver ions combined with UV-A and visible light irradiation. *Water Res.* **2008**, *42*, 356–362.

(51) McBain, A. J.; Ledder, R. G.; Moore, L. E.; Catrenich, C. E.; Gilbert, P. Effects of quaternary-ammonium-based formulations on bacterial community dynamics and antimicrobial susceptibility. *Appl. Environ. Microbiol.* **2004**, *70*, 3449–3456.

(52) Merkel, P. B.; Kearns, D. R. Radiationless decay of singlet molecular oxygen in solution. An experimental and theoretical study of electronic-to-vibrational energy transfer. *J. Am. Chem. Soc.* **1972**, *94*, 7244–7253.

(53) Merchat, M.; Spikes, J. D.; Bertoloni, G.; Jori, G. Studies on the mechanism of bacteria photosensitization by meso-substituted cationic porphyrins. *J. Photochem. Photobiol. B-Biol.* **1996**, *35*, 149–157.

(54) Costa, L.; Alves, E.; Carvalho, C. M. B.; Tome, J. P. C.; Faustino, M. A. F.; Neves, M. G. P. M. S.; Tome, A. C.; Cavaleiro, J. A. S.; Cunha, A.; Ahneida, A. Sewage bacteriophage photoinactivation by cationic porphyrins: a study of charge effect. *Photochem. Photobiol. Sci.* **2008**, *7*, 415–422.

(55) Rao, K. V. S.; Subrahmanyam, M.; Boule, P. Immobilized TiO_2 photocatalyst during long-term use: decrease of its activity. *Appl. Catal. B Environ.* **2004**, *49*, 239–249.

ES901501K